Gold and Base Metals Associated with Uranium Mineralization in some Lower Carboniferous Rock Units at Wadi Abu El Mogheirat area, Southwestern Sinai, Egypt

Osama Sallam, Abdalla Alshami, Abd Elhadi A. Abbas, Guibal Eric

Gold and Base Metals Associated with Uranium Mineralization in Some Lower Carboniferous Rock Units in the Wadi Abu El Mogheirat Area, Southwestern Sinai, Egypt

Osama R. SALLAM[1, *], Abdalla S. ALSHAMI[1], Abd Elhadi A. ABBAS[1] and E. GUIBAL[2]

[1] *Nuclear Materials Authority, Cairo, Egypt*
[2] *Institut Mines Telecom – Mines Alès, Centre des Matériaux des Mines d'Alès, University, Montpellier, France*

Abstract: The Lower Carboniferous sediments at Wadi Abu El Mogheirat consist of four stratigraphic formations, from base upwards: Um Bogma, El Hashash, Magharet El Maiah and Abu Zarab formations. The most-concentrated radioactive anomalies at Wadi Abu El Mogheirat are in the middle member of the Um Bogma Formation. The gibbsitic marl in this formation shows the highest uranium contents (around 710 ppm). Gibbsitic marl and black gibbsite of the middle Um Bogma Formation show higher enrichment in Co, Cu, Mn, Ni, Pb, Zn, U, V, Ce and Th. Black gibbsite contains the highest total rare earth elements concentration, especially in terms of LREEs, while gibbsitic marl contains the highest content of HREEs. Anomalous contents of gold at Wadi Abu El Mogheirat are recorded for the first time in the gibbsitic marl (content: 10.4 ppm), black gibbsite (2.8 ppm) of the middle member of the Um Bogma Formation and in the siltstones of the El Hashash Formation (0.6 ppm). Gibbsitic marl shows the presence of uranothorite, celestite, zircon, atacamite, barite, xenotime and rutile. These characteristic demonstrate that the middle member of the Um Bogma Formation constitutes a potential source for gold. This conclusion is reinforced by the potential to exploit other metals such as Co, Cu, Mn, Ni, Pb, Zn, U, V, Th and Ce as by-products.

Keywords: gibbsite, rare earth elements, Um Bogma

1 Introduction

Most of the gold deposits and mineralization in Egypt are located in the Eastern Desert area (Botros, 2015), which was extensively exploited in the Pharaonic times. In central Easter Desert of Egypt gold is associated to quartz/ carbonate veins; the hydrothermal activity explains the metamorphic source of gold ore deposits in relation with regional shear setting (Zoheir and Weihed, 2014). Remote sensing has been applied to identify the connections between several gold-bearing formations in this area; this allowed correlating surface structural elements, hydrothermal effects and lithological characteristics between different ore deposits (Gabr et al., 2015). Chemical analysis also demonstrated the association of gold with zinc in many analyzed samples. In this area, recent studies have shown the impact of carbonate alteration of ophiolithic ores; under hydrothermal conditions the remobilization of gold and sulfur caused the formation of gold deposit (Boskabadi et al., 2017). These hydrothermal alterations may explain not only the formation of these gold deposits but also its association to other base metals and calcareous mineralization (Helmy and Zoheir, 2015; Abdelnasser and Kumral, 2016).

Recently, the intensive geological exploration of Sinai area allowed identifying some promising anomalies for polymetallic ore deposits that contain not only base metals but also uranium and gold. The explored area (Wadi Abu El Mogheirat) is located close to Abu Zeneima (about 40 km in the ESE direction, Fig. 1a, this is like a "mirror" zone to the Central Eastern desert on the other side of the Gulf of Suez. Similarities may exist between the characteristics and origin of these different deposits belonging to the Arabian-Nubian shield (Bentor, 1985), although it is commonly accepted that Sinai is not a gold-mining area. The main cover in this area corresponds to Paleozoic sediments with concentrations of coal, copper, manganese, kaolin, glass sands, rare earth elements (REEs) and uranium. More recently, traces of thorium and gold have also been identified. The East Abu Zeneima area is made up of the Precambrian younger granites, overlain nonconformably by the Paleozoic succession.

The Paleozoic outcrops of Southwestern Sinai have been documented since the early 20th century: (Barron, 1907) reported three different series: (a) the Lower Sandstone Series (LSS), (b) the Carboniferous Limestone Series (CLS) (which was called the Um Bogma Formation by Weissbrod, 1969) and (c) the Upper Sandstone Series (USS). The Lower Sandstone Series was subdivided by Soliman and Abu El Fetouh (1969) into the Sarabit El Khadim, Abu Hamata and Adedia formations, also splitting the Upper Sandstone Series into the El-Hashash, Magharet El-Maiah and Abu Zarab formations.

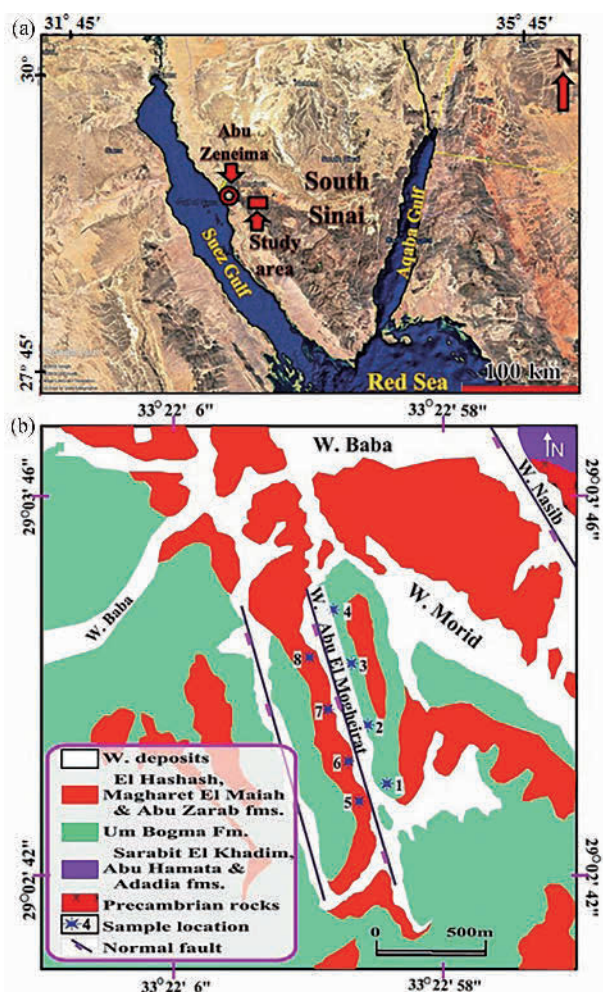* Corresponding author. E-mail: orsallam@yahoo.com

Fig. 1. (a) Landsat image showing location of the study area; (b) geological map of the Abu El Mogheirat area.

2 Geological Setting

The Wadi Abu El Mogheirat area is covered by rock exposures ranging from Precambrian to Paleozoic in age (Fig. 1b). Quartz diorites is the main component of the Precambrian rocks in this area, the Paleozoic sequences being subdivided into seven formations (arranged from oldest to youngest) as follows: Sarabit El Khadim Formation (Cambrian), Abu Hamata and Adedia formations (Cambro–Ordovician), Um Bogma, El Hashash, Magharet El Maiah and Abu Zarab formations (Lower Carboniferous).

Sarabit El Khadim Formation: Cross-bedded sandstones with a conglomerate layer, alternating with sandstones possessing a pinkish to brownish color, nonconformable with the underlying basement rocks.

Abu Hamata Formation: Conformably overlies and underlies the Sarabit El Khadim and Adedia formations, respectively. It is easily distinguished by its characteristic greenish color and lithology, which can be used as a marker in the field.

Adedia Formation: Made up of coarse- to fine-grained, pink to brown in color, hard ferruginous sandstones and

siltstones. The copper mineralization is recorded in the upper part of this formation. Also, there are Mn-Fe veinlets, in addition to some radioactive anomalous recorded in the Adedia Formation.

Um Bogma Formation: In the study area, the Um Bogma Formation unconformably overlies the Adedia Formation and underlies the El Hashash Formation. It is regarded as the most important Paleozoic rock unit in the study area, due to its content of uranium, Mn-Fe ore deposits and secondary copper mineralization. The formation exhibits a thickness of about 7 m and is classified from base to top as follows: The lower member rests unconformably on the Adedia Formation with a distinct contact, due to its different lithology. It is enriched by manganese and iron ores. This member exhibits three different lithological facies, including a) Mn-Fe ore (Fig. 2a), ferromanganese siltstones and silty shale facies with black, blackish-brown and reddish-brown colors; b) sandy dolostone facies, identifiable from its thick beds, pink color and occasional horizontal lamination; c) black carbonaceous shale, siltstone facies which is considered the most important facies for the uranium mineralization. The middle member is a yellow bed that consists mainly of marl and dolostone with some intercalated shale. The middle member is characterized through the distribution of highly radioactive anomalies, in addition to evaporite minerals such as gypsum, anhydrite and halite in fibrous and platy habits in the form of parallel veinlet's and/or intersection with bedding planes. Also, pockets of secondary copper mineralization, white and black gibbsite (Fig. 2b) were observed within the middle member of Um Bogma Formation with high radioactive anomalous. The upper member is composed of yellow, pink, and grayish crystalline dolostone and some sandstones.

El Hashash Formation: This consists of brownish, cross-laminated sandstones, intercalated with thin beds of shale and siltstone. Siltstones vary in color from white, yellow, red to violet (Fig. 2c).

Magharet El-Maiah Formation: It unconformably underlies the Abu Zarab Formation and overlies on the El Hashash Formation (Fig. 2d). The Magharet El-Maiah Formation consists of carbonaceous shale, sandstones, kaolin and claystone. There is a lateral variation in the lithology of this formation, i.e., the kaolin beds change laterally into carbonaceous shale in two horizons. Exploratory old mines for kaolin and coal were excavated parallel to the formation. It can be easily identified in the field through its distinctive physical characteristics.

Abu Zarab Formation: This formation consists of white, semi friable sandstones with siltstones and shale. It is considered to be the main source of glass sand ore in Sinai. The Abu Zarab Formation is locally capped by basaltic sheets.

Generally, the Um Bogma, El Hashash, Magharet El-Maiah and Abu Zarab formations are the only ones exposed at the Wadi Abu El Mogheirat. Wadi Abu El Mogheirat is affected by normal and horst faults (Fig. 2e and f) trending NW, with most of the observed radioactivity and mineralization being concentrated along these fault planes, which reveal the structural control of the mineralization. The lithology, structure and
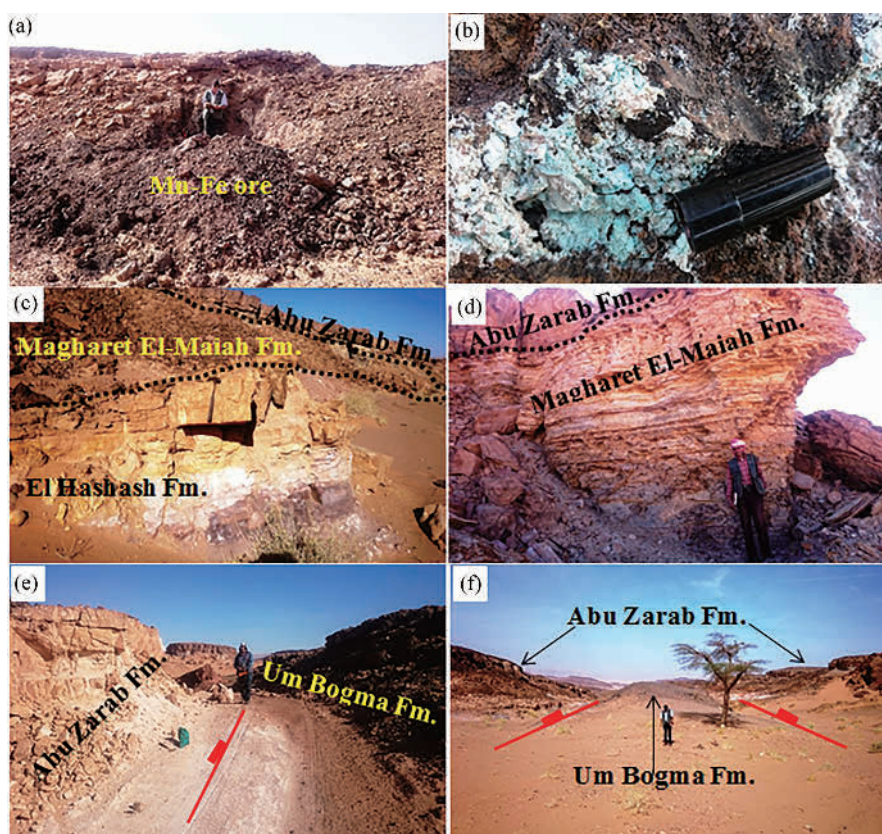
Fig. 2. Wadi Abu El Mogheirat; (a) Mn-Fe ore, lower Um Bogma Fm.; (b) pocket of secondary copper mineralization with white and black gibbsite, middle Um Bogma Fm.; (c) siltstones vary in color from white, yellow, red to violet, El Hashash Fm.; (d) Magharet El-Maiah Fm. underlines Abu Zarab Fm.; (e) normal fault.; and (f) horst faults.

topography played important factors in the localization of radioactive anomalies and mineralizations.

3 Materials and Methods

Field radiometric measurements were performed using a handheld gamma-ray spectrometer (Model Rs-230 BGO Super-Spec, Radiation Detection Systems AB, Backehagen, Sweden) (Fig. 2h) for the determination of eU (ppm), eTh (ppm) and K (%). The frequency for acquiring radiometric measurements was set to every 30 s.

Inductively coupled plasma optical emission spectrometry (720 ICP-OES Agilent Technologies, Santa Clara, CA, USA) was utilized for measuring uranium, trace and rare earth elements (REEs) (promethium was not analyzed). Samples were analyzed at the Central Laboratory Sector of the Egyptian Mineral Resources Authority (EMRA).

The mineral samples (crushed and sieved to 200 Mesh) were digested in teflon crucibles using 0.5 g of ground sample with 3 ml of perchloric acid, 5 ml of nitric acid and 15 ml of hydrofluoric acid. The mixture was covered with a glass lens and heated for 3 hours until digestion had been completed. In a second step, the glass lens was removed to evaporate silica tetrafluoride until complete evaporation. 5 ml of concentrated HCl was added to dissolve the solid residue; after drying through heating the solid was completely dissolved with 50 ml HCl aqueous solution (1:1 w/w); the volume was adjusted to 100 mL with distilled water, the concentration of metal ions being analyzed by ICP-QES (720 ICP-OES, Agilent Technologies, Santa Clara, CA, USA).

The determination of gold content required a further specific procedure; fire assay analysis was carried out at EMRA. 50 g samples (crushed and sieved to 200 Mesh) were fired in the presence of alkali fusion agents. More specifically, the ground sample was added to a mixture of (lead oxide), borax (sodium borate), sodium carbonate, flour, silica and silver in a ceramic crucible. The mixture was melted at 1000°C for 90 min; this step was followed by the cupellation of lead/gold/silver alloy at 900°C for 60 min. The resulting alloy (Ag/Au) was then dissolved with concentrated nitric acid and aqua regia under heat, in order to dissolve the gold; the solution was further analyzed by atomic absorption spectrometry (using a Savant AA spectrometer, GBC Scientific Instruments, Braeside, Australia).

The mineralogical composition of the samples required a preliminary conditioning of the samples. 3 to 5 kg of selected samples were crushed and sieved to collect a 0.074–0.5 mm (35–200 mesh) fraction. The sieved fraction was submitted to two separation steps: (a) densitometry separation using bromoform (Sp.G.: 2.85–2.89) (Quinif et al., 2006) and (b) magnetic separation

using a Frantz Isodynamic Magnetic Separator (S.G. Frantz Co., Inc, Tully town, PA, USA). For magnetic separation, the side slope was set at 5° and the forward slope at 20°, under an amperage of 0.5 A (Flinter, 1959).

Separated fractions were hand-picked using binocular microscope (Meiji, Japan), then analyzed with an Environmental Scanning Electron Microscope ESEM (XL30-ESEM, Philips, FEI, Thermo Fisher Scientific, Hillsboro, OR, USA) associated with an attached energy dispersive X-ray spectrometer (EDX) unit. Analysis was operated with the following parameters: 25–30 kV accelerating voltage, 1–2 mm beam diameter and 60–120 s counting time. Polished sections were specifically analyzed using a Quanta FEG200 (FEI-France, Thermo Fisher Scientific, Merignac, France) coupled with an Oxford Inca 350 EDX micro analyzer (Oxford Instruments France, Saclay, France) at the C2MA at IMT–Mines Ales.

4 Results and Discussion

4.1 Radioactivity

The radioactivity was recorded in several areas in Sinai. The most notable result was recorded in the Paleozoic rocks, specifically in the Um Bogma Formation. Most of the radioactive anomalies are concentrated with a definite stratigraphic horizon among them; the most significant uranium occurrences are located in the middle member of the Um Bogma Formation in the study area.

According to the radiometric measurements of the anomaly locations in the study area (Table 1) most radioactive anomalies are concentrated in the middle member of the Um Bogma Formation. More specifically, the gibbsitic marl shows the highest eU contents ranging between 310 ppm and 360 ppm with an average of 333.6 ppm, while varying from 227.3 ppm to 280 ppm with an average of 261.6 ppm in the black gibbsite. Siltstones of the El Hashash Formation show low eU contents relative to the Um Bogma Formation, ranging between 23.7 ppm and 44.8 ppm. The black shale of the Magharet El-Maiah Formation shows much lower eU contents, varying from 17.5 ppm to 39.6 ppm with an average of 30.9 ppm.

When uranium content was measured chemically for the studied anomalous facies (Table 1), the gibbsitic marl of the Um Bogma Formation showed the highest uranium content ranged between 412 ppm and 717.4 ppm with an average of 698.3 ppm, while the black gibbsite varied from 138.6 ppm to 149.8 ppm with an average of 144 ppm. Siltstones of the El Hashash Formation had as high uranium content, ranging between 310 ppm and 340 ppm with an average of 321.2 ppm, while the black shale of Magharet El-Maiah varied from 50 ppm to 60 ppm with an average of 54.6 ppm.

The eU/eTh ratio is a very important geochemical index for U migrating in or out, being approximately constant within the same rock type or geological unit in a relatively closed environment. The Clark value for eU/eTh in the sedimentary rocks is equal to 1 (Clark et al., 1966). The eU/eTh ratio of the studied anomalous facies is much higher than the Clark value, in which the average ratio reaches 7.0 and 13.3 for the gibbsitic marl and the black gibbsite of the Um Bogma Formation respectively, while

Table 1 Radiometric and chemical measurements of the anomalous samples, Wadi Abu El Mogheirat area

Age	Fm.	Lithofacies	eU (ppm)	U (ppm)	eTh (ppm)	K (%)	eU/eTh	U/eU
Lower Carboniferous	Magharet El-Maiah	Black shale	33.5	60.0	12.1	0.3	2.8	1.8
			30.1	53.2	9.7	0.9	3.1	1.8
			25.7	55.7	11.3	1.5	2.3	2.2
			39.2	50.0	19.2	0.3	2.0	1.3
			17.5	51.5	13.1	0.1	1.3	2.9
			39.6	57.3	16.8	1.2	2.4	1.4
		Max.	39.6	60.0	19.2	1.5	3.1	2.9
		Min.	17.5	50.0	9.7	0.1	1.3	1.3
		Average	30.9	54.6	13.7	0.7	2.3	1.9
	El Hashash	Siltstones	26.2	340.0	17.2	2.3	1.5	12.97
			33.5	325.2	25.3	1.9	1.3	9.71
			37.9	327.6	15.1	1.7	2.5	8.64
			35.2	310.0	11.7	2.1	3.0	8.81
			23.7	315.1	9.2	3.2	2.6	13.30
			44.8	311.3	13.0	1.0	3.4	6.95
		Max.	44.8	340.0	25.3	3.2	3.4	12.97
		Min.	23.7	310.0	9.2	1.0	1.3	6.95
		Average	33.55	321.2	15.25	2.03	2.4	10.06
	Middle Um Bogma	Gibbsite marl	360.0	717.4	42.5	1.3	8.5	1.99
			345.6	412.0	50.3	0.9	6.9	1.19
			320.4	615.2	47.8	1.8	6.7	1.92
			310.5	508.6	41.5	0.6	7.5	1.64
			310.0	503.0	53.2	1.1	5.8	1.62
			355.2	716.9	56.5	1.2	6.3	2.02
		Max.	360.0	717.4	56.5	1.8	8.5	2.02
		Min.	310.0	412.0	41.5	0.6	5.8	1.19
		Average	333.6	698.3	48.6	1.2	7.0	1.73
		Black gibbsite	280.0	149.8	22.8	0.9	12.3	0.51
			277.3	146.5	19.5	0.7	14.2	0.53
			250.9	139.1	17.3	1.8	14.5	0.55
			260.7	144.7	28.4	0.4	9.2	0.55
			227.3	138.6	15.6	1.3	14.6	0.61
			273.4	145.3	18.2	1.7	15.0	0.53
		Max.	280.0	149.8	28.4	1.8	15.0	0.61
		Min.	250.9	138.6	15.6	0.4	9.2	0.53
		Average	261.6	144.0	20.3	1.1	13.3	0.55

reaching 2.3 and 2.4 for the siltstones of the El Hashash and the black shale of the Magharet El-Maiah formations respectively. This indicates that the studied anomalous facies have experienced inward migration (leaching) of uranium from the surrounding country rock units, which is finally concentrated in fractures and fault planes. The presence of clay and iron minerals in addition to the organic matter play an important factor in the capture of uranium and the deposition of that metal in the fractures (Baioumy et al., 2012). The alteration of rocks contributes to U mobility and leads to the concentration of radioelements in fractures and faults (El Aassy et al., 2011). The hydrothermal conditions strongly control the migration of heavy metals and the deposition of Mn-Fe mineralization (Al-Ateeq et al., 2013).

The D-factor represents the ratio of the chemically measured uranium content to the radiometrically measured uranium (D: U/eU). When this factor is more or less than unity; it indicates that the system is in a disequilibrium state, which could be due to the addition or removal of U (Hansink, 1976).

The chemical analysis of samples systematically shows higher values than the radiometric measurements: the D-factor is around 1.73 for gibbsitic marl (in the Um Bogma Formation), 10.09 for siltstones of the El Hashash Formation and 1.9 for the black shale of the Magharet El-

Maiah Formation. These indicate an addition of recent uranium, indicating that these facies are in a state of disequilibrium. A completely different trend is observed when considering black gibbsite from the middle Um Bogma Formation (deeper layers); indeed, in these rocks, the D-factor remains close to 0.55: uranium was leached from these layers, probably transported away and finally deposited in the fractures of surrounding formations. Similar phenomena have been reported for U mineralization in Eastern Desert deposits (Dawood et al., 2014). Figures 3-4 show the correlation of eU, eTh and U (chemical measurements) with the K (%) content in the mineral samples. The evolution of the Clark coefficient and D-factors with K (%) content is also presented on Fig. 5–6. The grouping of data is also correlated to the corresponding geological formations and lithofacies. The radiometric measurements can be easily correlated in the different lithofacies and the content of K (%) hardly changes with the relative values of eU and eTh (Fig. 4).

There is no continuity in terms of U content between the different geological layers: Figure 5 shows that the relative richness in U decreases in the following pattern: gibbsite marl (middle Um Bogma Formation) > siltstones (El Hashash Formation) > black gibbsite (middle Um Bogma Formation) > black shale (Magharet El-Maiah Formation). The Clark coefficient (i.e., eU/eTh) shows a progressive decrease from black gibbsite to black shale and siltstone lithofacies (lower layers to higher layers); this means that the deeper layers were more affected by the alteration of U-bearing rocks (probably due to epigenetic effects). The D-factor varies in the opposite direction: the upper layers are more significantly affected by the mobility of uranium (leaching and subsequent deposition in fractures and faults). Two main hypotheses can be proposed for explaining this selective localization of uranium: (a) the epigenetic deposition of radioelements during lithification and (b) the leaching of the radioelements (in a second step), followed by their transport and re-precipitation in fractures and faults. The secondary ascending hydrothermal solutions transport the radioactive minerals to deposit primarily along fractures and faults.

4.2 Geochemistry
4.2.1 Base metals and uranium/thorium

The chemical analysis of the selected samples (#1-8) collected in four different lithofacies (belonging to three geological formations) is summarized in Table 2 (Figs. 7–8). Gibbsitic marl and black gibbsite from the middle Um Bogma Formation show high enrichment in Co, Cu, Mn, Ni, Pb and Zn (levels exceeding 1000 ppm, with even more than 10000 ppm for Mn). Mn-Fe ore constitutes an important fraction of rocks in the Um Bogma Formation (Kora et al., 1994; Shaaban et al., 2005; Khalifa and Arnous, 2012; Rabeh, 2016).

The metal content in black gibbsite is generally higher than in gibbsitic marl, with the exception of Zn (a similar order of magnitude) along with Co and Cr (higher content in gibbsitic marl) (Fig. 7). For siltstones (El Hashash Formation) and black shale (Magharet El-Maiah Formation) the levels of metal content are much lower (below 450 ppm), with the exception of Nb and Zr (only

in black shale, with levels of 300–450 ppm). It is noteworthy that metal content is generally higher in the black shale than in the siltstones of these geological
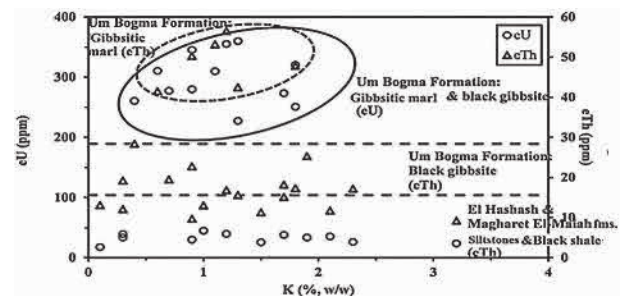

Fig. 3. Correlation between K content of selected samples and both eU and eTh radiometric measurements (and geological formations or lithofacies).
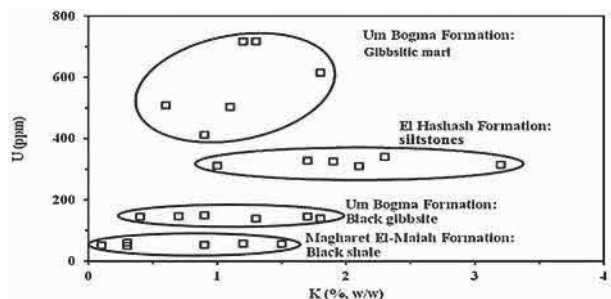

Fig. 4. Correlation between K content of selected samples and U chemical measurements (and geological formations or lithofacies).
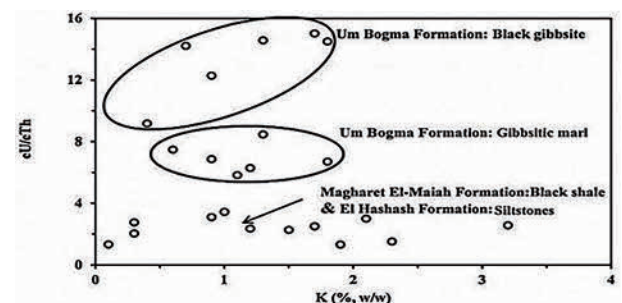

Fig. 5. Correlation between K content of selected samples and the Clark coefficient (eU/eTh) (and geological formations or lithofacies).
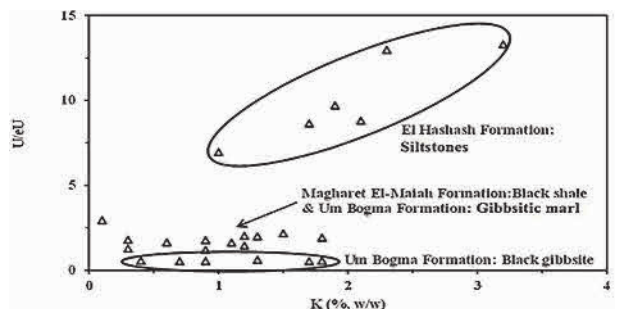

Fig. 6. Correlation between K content of selected samples and the D-factor (U/eU) (and geological formations or lithofacies).

formations.

Thorium presence is limited in superficial layers (siltstones and black shale) with concentrations lower than 14 ppm; in contrast, the middle Um Bogma Formation shows much higher content (i.e., 154–178 ppm for gibbsitic marl and up to 335–357 ppm for black gibbsite lithofacies). Uranium (Table 1) is also predominantly detected in the gibbsitic marl (703–717 ppm) when compared to the black gibbsite (i.e., 139-150 ppm). However, contrary to Th distribution, substantial levels of U are detected in the El Hashash siltstones (i.e., 310–340 ppm) and to a lower extent in the Magharet El-Maiah black shale (i.e., 50–60 ppm). This is indicative of the presence of secondary mineralization due to alteration, metal migration and local sedimentation/precipitation
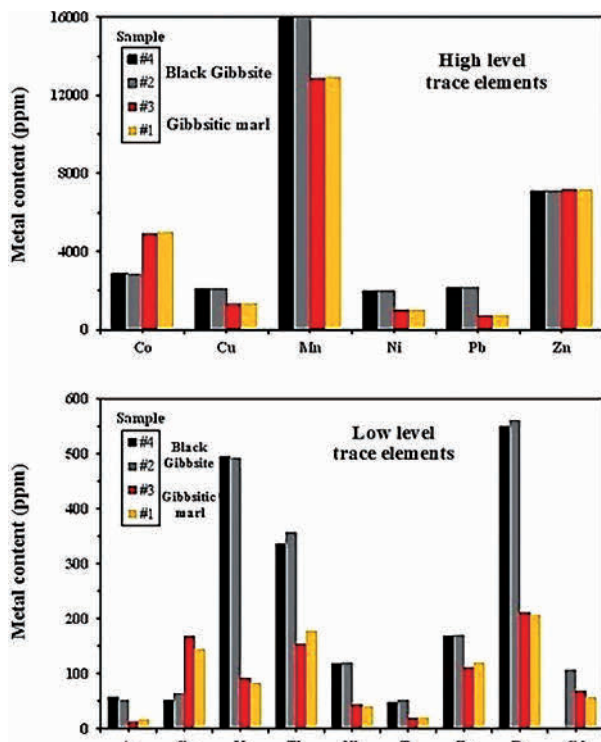

Fig. 7. Metal content in samples collected from the middle member of the Um Bogma Formation (black gibbsite and gibbsitic marl) (trace elements).
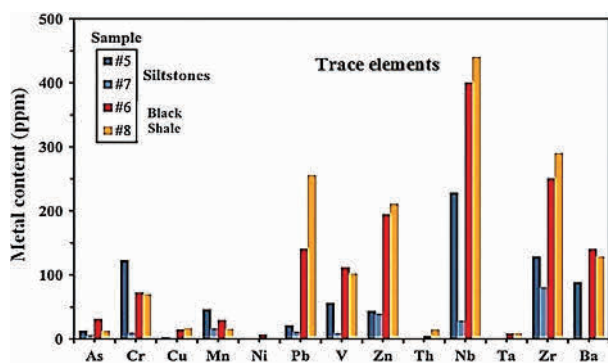

Fig. 8. Metal content in samples collected from the El Hashash Formation (siltstones) and the Magharet El-Maiah Formation (black shale).

(Abu-zeid et al., 2017).

4.2.2 Rare earth elements (REES)

The presence of rare earth elements requires particular attention (Table 3, Fig. 9a–c). The lithofacies can be ranked according to their total rare earth content: siltstones (El Hashash Formation) [38–90 ppm] << black shale (Magharet El-Maiah Formation) [248–252 ppm] << gibbsitic marl [899–929 ppm] << black gibbsite [1776–1824 ppm] (Um Bogma Formation). The greatest part of these REEs content is cerium: around 42%–46% for Magharet El-Maiah and El Hashash formations, respectively, around 59% for gibbsitic marl and up to 86% for black gibbsite of the Um Bogma Formation. Among the most representative REEs in the samples collected in the middle Um Bogma Formation, apart from Ce, are: Nd (in the range 56–136 ppm), Pr (in the range 40–64 ppm), Gd (in the range 36–48 ppm), Dy (19–28 ppm) and Sm (15–27 ppm).

Table 2 Chemical analysis of trace elements (ppm) from the anomalous samples, Wadi Abu El Mogheirat area

Formation	Middle Um Bogma				El Hashash		Magharet El-Maiah	
Rock type	Gibbsitic marl		Black gibbsite		Siltstones		Black shale	
Sample #	1	3	2	4	5	7	6	8
As	16.5	12.5	52	57	12.5	5.3	31	12.1
Cd	57	68	107	u.d.	u.d.	u.d.	u.d.	u.d.
Co	4980	4899	2822	2853	u.d.	u.d.	u.d.	u.d.
Cr	145	168	64	52	122	9.2	72	69
Cu	1346	1329	2072	2055	2.18	u.d.	14.2	16.1
Mn	12926	12874	15976	15873	45.7	16.1	29.2	14.9
Ni	1005	1011	1949	1953	0.26	u.d.	5.8	1.1
Pb	724	718	2141	2128	1	11	140	256
V	83	92	492	495	56	9.1	111	12
Zn	7158	7164	7072	7061	43.1	38.9	194.0	210.6
Th	178	154	357	335	u.d.	u.d.	4.2	14.0
Nb	40	43	120	118	228	28	400	440
Ta	20	19	52	47	u.d.	u.d.	8	8
Zr	120	111	170	168	128	80	250	290
Ba	206	211	560	549	88	u.d.	140	128

u.d.: under detection limit.

Table 3 Chemical analysis of rare earth elements (ppm) from the anomalous samples, Wadi Abu El Mogheirat area

Formation	Middle Um Bogma				El Hashash		Magharet El-Maiah	
Rock type	Gibbsitic marl		Black gibbsite		Siltstones		Black shale	
Sample #	1	3	2	4	5	7	6	8
La	65.9	58	1.65	1	18.7	7.9	44.7	46.8
Ce	543.8	533.7	1562	1543	37.9	16.9	115.7	112.9
Pr	43.14	39.7	53.7	63.7	4.5	2.13	13.1	10.8
Nd	132.5	135.6	75.4	55.8	13.3	5.7	42.6	36.18
Sm	26.5	21.3	15	17.5	2.3	0.66	9.64	9.53
Dy	25.28	19.2	28.16	19.7	2.3	0.67	4.6	5.07
Er	12.8	13	10.5	11.3	2.9	0.56	5.44	6.12
Eu	7.5	6.5	6.8	7.1	0.5	0.19	1.7	1.39
Gd	46	48.1	47.4	35.8	4	1.8	8.1	6.18
Ho	2.75	2.21	2.2	1.7	0.0044	u.d.	0.106	0.086
Lu	1	0.9	3.2	2.1	0.58	0.28	0.688	3.92
Tb	7.5	6.6	7.2	7	1.44	0.4	2.2	2.43
Tm	4	2	u.d.	u.d.	u.d.	u.d.	u.d.	u.d.
Yb	10.5	11.8	11.7	9.7	1.7	0.5	3	3.3
LREEs	811.8	788.3	1707	1681	76.7	33.29	225.7	216.2
HREEs	117.3	110.3	117.2	94.4	13.4	4.4	25.8	28.5
ΣREEs	929.2	898.6	1824	1776	90.1	37.7	251.6	244.7
L/H	6.9	7.2	14.6	17.8	5.7	7.6	8.7	7.6

u.d.: under detection limit.

The contents are in the same order of magnitude in the two lithofacies of this geological formation. The case of La is remarkable: gibbsitic marl contains between 58 and 66 ppm of lanthanum, while its content decreases below 2 ppm in black gibbsite. The REEs can be classified in two groups: light REEs (LREEs) with atomic number below 63 (i.e., up to and including samarium) and heavy REEs (HREEs) with atomic number higher than 62 (i.e., beginning with Eu). This separation remains debatable in the literature. In most cases, the LRREs/HREEs ratio varies between 5.7 and 8.7, except for black gibbsite where it ranges between 14.6 and 17.8. This confirms the anomalies of the mineral fingerprint of this lithofacies within this specific geological formation.

The REEs distribution is frequently normalized using models associated with both chondritic abundance (Schmitt et al., 1964) (Fig. 9a) and North American Shale Composite abundance (NASC) (Gromet et al., 1984, Fig. 9b; Haskin et al., 1968, Fig. 9c). These simulations are summarized in Figs. 9a–c for selected lithofacies from the different geological formations. The profiles are relatively stable, with regard to the normalized values of the REEs; the curves roughly follow the same trend independent of the type of geological formation.

The normalized profile against chondrite (Fig. 9a) shows a substantial enrichment of the REEs. The main anomalies are identified for holmium and cerium. Indeed, in siltstones and black shale, negative anomalies are observed for Ho, while positive anomalies can be seen for gibbsitic marl and black gibbsite (a similar positive anomaly, but to a lesser extent, is observed for praseodymium). Cerium anomalies are generally associated with laterization effects and oxidative/reductive conditions during the degradation of primary rocks (Al-Khirbash et al., 2014). The impact of oxidative conditions on REE distribution can be assessed by the effect of microbial activity in altered zones (Censi et al., 2014).

The concentration of rare earth elements (such as uranium) into preferential geological layers was correlated to lithological characteristics such as porosity and permeability: the presence of impermeable stratigraphic levels contributes to the accumulation of mobile metals (Abu-zeid et al., 2017).

4.2.3 Gold

Many studies on gold exploration in Egypt have focused on the Eastern Desert; on the other hand, Sinai is not considered a promising area for Au exploitation. The early exploration programs of the Geological Survey of Egypt concluded that gold in Sinai was essentially confined to quartz veins and carbonated ultramafics (appearing as listwaenite) (Khalid and Oweiss, 1995b). In Pharaonic times, gold was extracted in the Eastern Desert of Egypt from quartz veins and placers. In some specific local areas, small-tonnage mines exploited gold, which occurred as dispersed grains or was associated with sulfides in quartz veins along shear planes at Wadi Kid (Surour et al. 2003), where relatively high levels of gold (up to 16.5 ppm) appeared in altered rocks (Khalid and Oweiss, 1995a). Minerals bearing Ag and Au (under the form of uytenbogaardtite and furutobeite) were identified in the
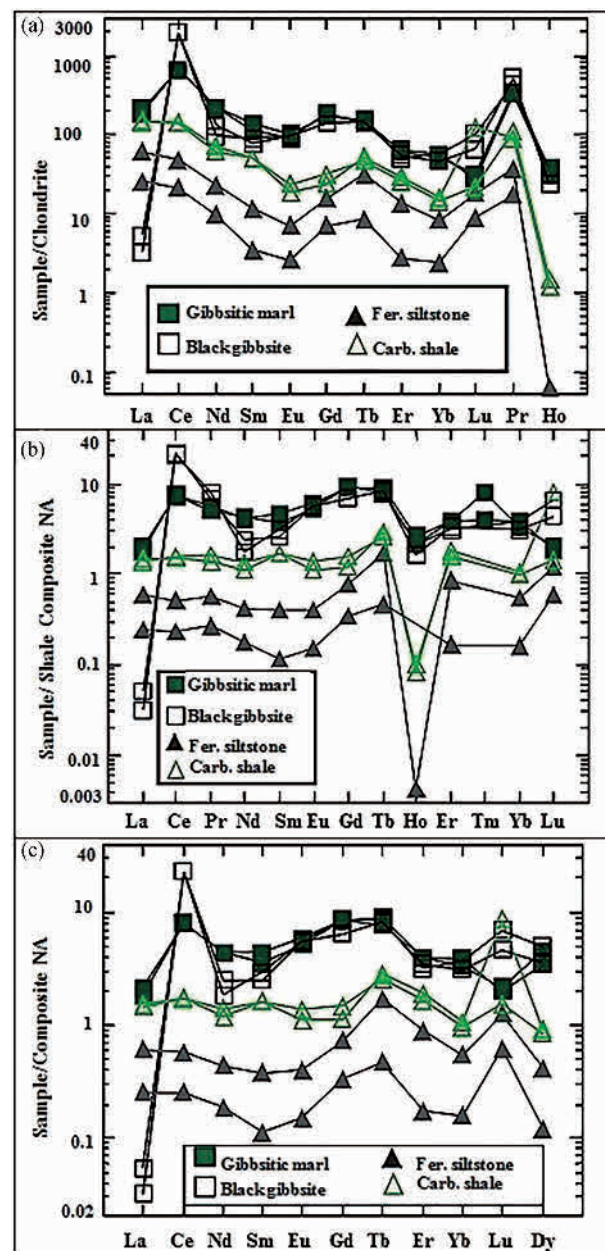

Fig. 9. (a) Rare earth element distribution pattern of the anomalous samples normalized to chondrite (Schmitt et al., 1964); (b) rare earth element pattern of the anomalous samples normalized with NASC (Haskin et al., 1968); (c) rare earth elements pattern of the anomalous samples normalized with NASC (Gromet et al., 1984).

Table 4 Gold concentrations (ppm) in different lithofacies in the Wadi Abu El Mogheirat area

Formation	Lithofacies	Semple #	Au (ppm)
Magharet El-Maiah	Black shale	6	u.d.
El Hashash	Siltstones	5	0.6
Middle Um Bogma	Black gibbsite	2	2.8
	Gibbsitic marl	1	10.4

u.d.: under detection limit.

lower member of the Um Bogma Formation in the El Sheik Soliman area (to the south of the study area)

(Sallam et al., 2014). It is commonly accepted that sedimentary basins that contain paleo-placers may have been formed under tectonic regimes that existed only during the Proterozoic era (Mitchell and Garson, 1981), such as the gold bearing Taba conglomerate (Hassan et al., 2013).

Table 4 summarizes the evaluation of gold traces in the samples. Gold is either undetectable (in the black shale of the Magharet El-Maiah Formation) or occurs only at a very low content (below 1 ppm in the siltstones of the El Hashash Formation) in the upper geological layers; a few higher contents are measured in the samples collected in the middle Um Bogma Formation, especially in the gibbsitic marl (10.4 ppm vs. 2.8 ppm in black gibbsite lithofacies).

This is consistent with the levels (i.e., around 9.7 ppm) reported by Alshami (2019), who observed a progressive decrease in the gold content of Um Bogma mineralization, correlated with the time of deposition during the Cambrian -Ordovician sedimentary period (Alshami, 2019). The levels of gold are consistent with those reported in volcanic and subvolcanic rocks of the Wadi Abu Khushayba area (Jordan) (Al-Hwaiti et al., 2010). The same order of magnitude was also found for non-altered rocks and altered rocks samples collected in the El-Hoteib area (in the south eastern Desert, Egypt) (Gabr et al., 2015). The alteration phenomena were furthermore associated with the formation of low-grade gold deposits in the central Eastern Desert (Egypt): gold content varied between 1.9 and 4.9 ppm in quartz veins and decreased to 1.4-2.8 ppm in listwaenite alteration rocks (Salem et al., 2014).

4.2.4 Lithofacies–main characteristics of metal distributions

In the gibbsitic marl the REEs represent about 629–900 ppm with about 87% of LREEs (including up to 89% for Ce) (Table 4): there is a strong enrichment of LREEs in this geological formation (the L/H ratio increases up to 14 –18 compared to 6–9 for other lithofacies). Figures 9a–c show that these REEs are almost equally enriched when considering the normalized plots against chondrite and North American Shale Composite (NASC). Figure 7 shows that the samples contain high levels of Mn (above 12000 ppm); this is logically associated with the Fe-Mn ore component of Um Bogma mineralization. There are also significant amounts of Zn (up to 7000 ppm) and Co (close to 4900 ppm); other high level traces consist of Pb, Ni and Cu. Lower levels of base metals were identified: essentially Ba (around 200 ppm), V (close to 100 ppm) and Th (around 160 ppm, consistent with U-enrichment and radiometric measurements, see above). This is also the geological formation where the gold level is the highest (around 10 ppm) and the levels of As are relatively low (12–17 ppm).

The metal contents in the black gibbsite layer were consistent with those found in the gibbsitic marl though usually higher; especially for Mn (up to 14000 ppm), Ba (550 ppm), Th (up to 350 ppm), V (remarkably increased to 500 ppm) and Nb (up to 120 ppm). Gold content decreased to 2.8 ppm, while arsenic increased to 52–57
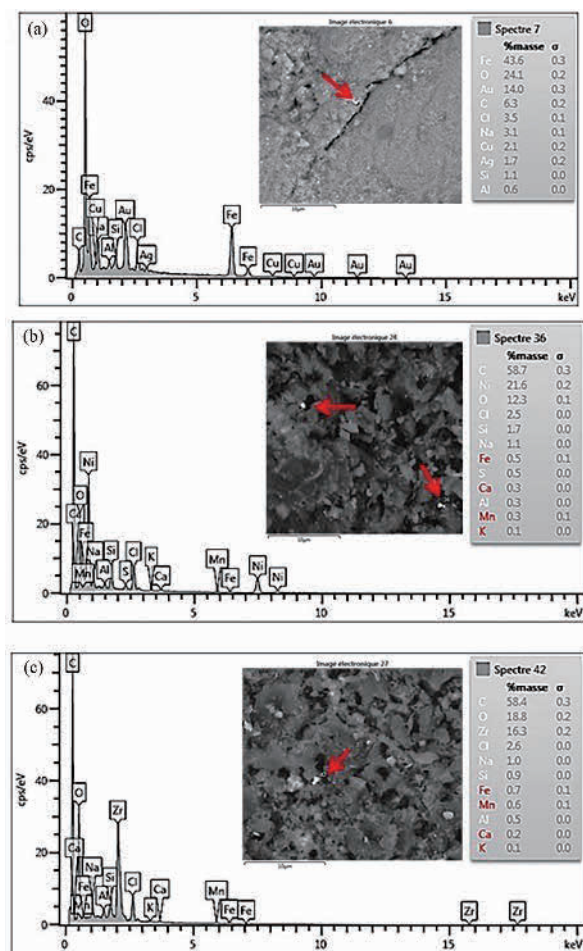

Fig. 10. EDX and BSE image images showing: (a) Au/Cu/Ag, (b) Ni, (c) Zr rich mineral objects (spots identified by arrows).

ppm: this means that there is no direct correlation between Au and As; in other words, Au mineralization is probably not associated with the occurrence of arsenopyrite. In this lithofacies, the REE content increased up to 1800 ppm, with LREEs representing up to 94% of total REEs (and Ce up to 86%). The positive Ce anomaly is confirmed by Figs. 10a–c, while La shows a substantial deviation from the general trend, with a negative anomaly.

The metal contents in siltstones were remarkably low, when compared with the levels observed in the other lithofacies: REEs represented less than 90 ppm, with base metals being consistently below 100 ppm. This is depicted in Fig. 9a–c: normalized plots (against both chondrite and NASC) show much lower enrichment in REEs compared to gibbsitic marl and black gibbsite lithofacies. The holmium anomaly is detected, but with a dramatic decrease in content (in fact undetectable in one of the two samples). Abu-zeid et al., (2017) correlated the highest radiometric activity and content of REEs in highly porous and permeable sandstones compared with the siltstones with their porous and permeable structure.

The black shale lithofacies shows an intermediary trend: total REE content reaches up to 250 ppm (about 89% of LREES, including 46% of Ce). In this lithofacies, the

normalized plots (Figs. 9a–c) allow the identification of the negative Ho anomaly, while the enrichment factor is remarkably stable for the other REEs. The base metal contents are also higher compared to the siltstone layer, but is significantly lower than for the samples collected in the Um Bogma Formation. The most representative trace elements are Ba (around 130 ppm), Zn (around 200 ppm) and Pb (in the range 140–210 ppm). However, the most surprising observation is the high level of neodymium (Nd) in this geological layer (in the range 400–440 ppm).

The enrichment of REEs (and especially LREEs) can be explained by the carbonaceous nature of the mineralogical structure of the Um Bogma Formation. This is associated with the deposition of organic matter under continental and fluviomarine conditions, an effect that is due to the direct adsorption of metal ions on to this organic matter, or is due to the indirect effects on the physico-chemical conditions that promote the reduction or precipitation of metal ions into the sediments. This can be followed by further migration and re-deposition due to variations in physico-chemical conditions and permeability properties. The accumulation of organic matter in sediments is frequently associated with the enrichment of rocks with sulfur and iron (Shata and Mira, 2010).

Field observations and laboratory characterization of samples confirm that the middle member of the Um Bogma Formation can be considered as a potential source for gold, associated with other exploitable metals that can be used as secondary resources, such as U, Th, Ce, Zn, Co, Cu, Mn, Pb and V.

In general, the probable origin of the gold, uranium, base metals and REE is related to the epigenetic concept, in which the secondary ascending hydrothermal solutions transport the metals through the network of fractures and the change of physico-chemical environment causes the deposition of metals along the fractures and faults. This is in addition to the leaching concept, in which the Au, U, base metals and REE in the surrounding rock units has been transported by means of weathering, especially circulating water, until it is finally captured and deposited by the organic matter in addition to the iron oxides present in the studied facies.

4.3 Mineralogy

The samples collected from the gibbsitic marl layer are characterized by the highest relative contents of U and Au. They were further characterized by mineralogical observation on polished sections and analysis using ESEM and EDX analysis. Figures 10–12 allow identifying specific mineralized objects containing a broad range of
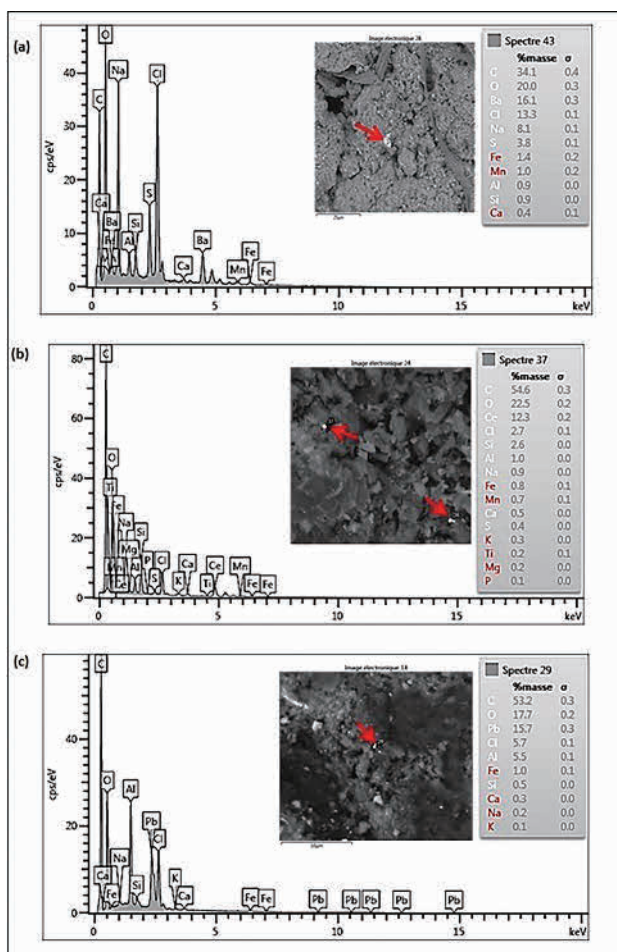

Fig. 11. EDX and BSE image images showing: (a) Ba, (b) Ce, (c) Pb rich mineral objects (spots identified by arrows).
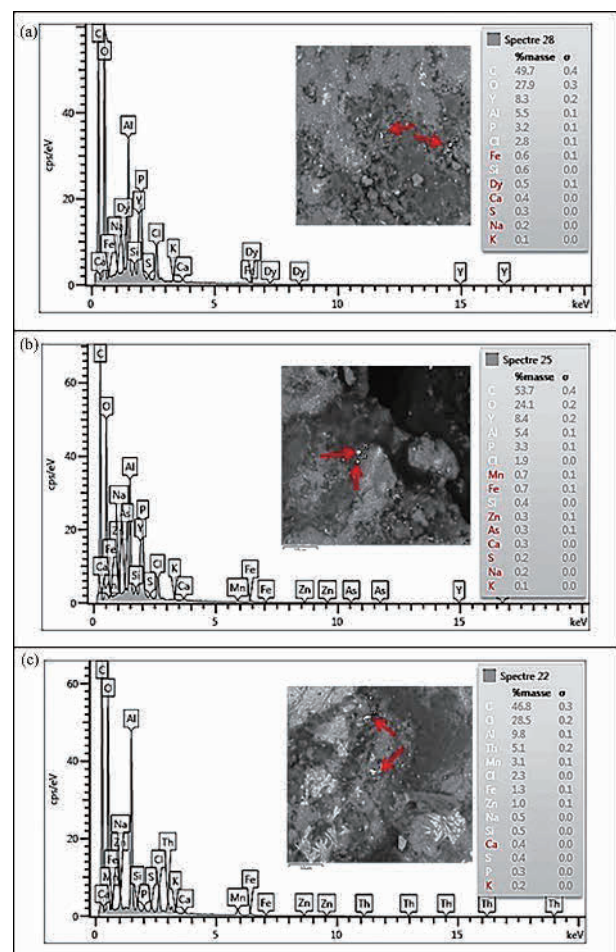

Fig. 12. EDX and BSE image images showing: (a) Y, Dy and S, (b) Y, Mn, Zn and As, (c) Th, Mn, Fe, Zn and S rich mineral objects (spots identified by arrows).

elements significantly present in the samples: Fe, Au, Cu, Ag, Ni, S, Mn, Zr, Co, Ba, Ce, Pb, Y, P, Dy, Zn, As and Th. In the sedimentary succession of Um Bogma and Adedia formations several important mineral assemblage associations were reported including: coffinite, marcasite, zincochromite, sodium meta-autunite and pucherite, in addition to proper Mn-Fe structural deposit (El Akeed et al., 2014). Most of the minerals analyzed at the surface of the polished sections are associated to a relatively high content of C (ranging between 38 and 59 wt%): this is directly associated to the carbonaceous nature of the sedimentary rocks. Figure 11a shows a different trend in the identification of Au/Ag/Cu mineralization: C content does not exceed 3.5 wt%, while iron oxide predominates (Fe content close to 44 wt%).

Uranium minerals in sedimentary rocks can exist in different forms; they are associated with oxides, oxyhydroxides, carbonates, silicates, phosphates, arsenates, vanadates, molybdates and sulfates (Alshami, 2003; Shata, 2006; Shata and Mira, 2010; Shata, 2013). They are frequently found in Paleozoic sediments of southwestern Sinai in Mn-Fe ores, claystones, siltstones, gibbsites, dolostones, marls and shales of the Um Bogma Formation.

The combination of geological and lithological data, SEM and EDX observations, as well as chemical analyses, allows the identification of the main minerals associated with these valuable metals. Figure 13 shows some examples of these minerals, including the results of their EDX analysis. Uranothorite (Fig. 13a) is a uranium-thorium silicate, characterized by a yellow to yellowish brown color, with a crystallographic structure corresponding to subhedral-to-unhedral shapes with rounded corners. Uranium and thorium contents approach 15.4% and 55.7% (wt%), respectively. Impurities are also observed such as Y, Zr, Fe, Al, Ca, V and P. This is consistent with the conventional contents reported in the literature (Heinrich 1958). Celestite (strontium sulfate, Fig. 13b) occurs as prismatic crystals, the EDX analysis showing the presence of Cs, K, Fe and Al impurities.

Fig. 13c shows a zircon crystal (zirconium silicate); yellowish to reddish-brown colored, with a crystallographic structure with characteristics between euhedral and subhedral. It is noteworthy that the EDX analysis shows the presence of Fe, Ca, K, Al elements and some indices of Hf and U. The metamictization of zircon crystals is associated with the presence of U and/or Th within the crystal structure. High levels of uranium may cause the destruction of zircon structure due to energy dissipation during the decay of the radioactive elements. In the present case, the level of uranium was low enough for the crystallized structure of zircon to be maintained. Figure 13d permits the identification of a relatively rare form of oxychloride of copper (i.e., atacamite), which is usually formed during the oxidation or weathering of primary copper minerals under arid climates.

Fig. 13e confirms the presence of barium in the Um Bogma samples: barite (barium sulfate) appears as white, rounded, pitted and grooved grains; it is noteworthy that strontium also appears as an impurity. Figure 13f shows an yttrium phosphate crystal (yellow to brownish yellow colored grains): xenotime is a typical mineral appearing in sedimentary rocks during diagenetic phases. The EDX analysis shows that many other REEs are associated with Y and that impurities are presents, such as Fe, Si, Al, Pb and Ca. The presence of high base metal contents in mineral samples collected in the Um Bogma Formation at Wadi El Sahu and Ramlet Hemiyir (localized respectively at the north and northeast of the Wadi Abu El Mogheirat area) has been correlated with xenotime (and with Mn-Fe ore deposits, to a lesser extent) (El Kammar et al., 1997). Figure 13g shows a rutile crystal (TiO_2), characterized by an euhedral structure; and reddish brown to deep brown color. Some indices of Al, Si and Cl are also identified. Rutile is usually generated under high temperatures and pressures in metamorphic and igneous rocks. This means that the different minerals identified in the Um Bogma Formation reflect a wide range of genetic conditions: the deposit is characterized by a mix of different rocks, with successive metal migration and deposition under changing environments.

5 Conclusion

The Wadi Abu El Mogheirat area is affected by normal fault trending NW–SE; most of the radioactive anomalies and mineralization indices are specifically concentrated along the planes of these faults. Radiometric field measurements showed that radioactive anomalies are concentrated in the Um Bogma Formation: the highest eU measurements were assigned to the gibbsitic marl (i.e., 360 ppm). The ore deposit is in disequilibrium, as shown by the higher levels of uranium in ore samples (i.e., 703–717 ppm) compared to the radiometric measurements.

The enrichment of the deposit in base metals follows the same trend with higher mineralization of metals such as Co, Cu, Mn, Ni, Pb, Zn and V in the middle Um Bogma Formation. REEs are also significantly enriched: black gibbsite contains the highest REE content (up to 1800 ppm mainly consisting of LRREs; i.e., about 94%, including Ce that represents about 86% of total REEs). Gibbsitic marl is less enriched: the content in REEs is close to 900–930 ppm (87% of LREEs, including 59% Ce). The carbonaceous rocks (rich in organic matter) in the Um Bogma Formation facilitate the direct binding of metal ions or the physico-chemical deposition of these metals.

The analysis of gibbsitic marl reveals surprisingly high levels of gold (i.e., 10.5 ppm); lower levels were detected in the black gibbsite (i.e., 2.8 ppm), while other lithofacies show negligible amounts of gold. The gold content sharply decreases in layers according to the time of deposition during the Carboniferous sedimentation era.

The probable origins of the gold, uranium, base metals and REE are related to many concepts. The epigenetic concept in which the secondary ascending hydrothermal solutions transport the metals through the network of fractures and the change in physico-chemical environment causes the deposition of metals along the fractures and faults. Furthermore, it is not possible to reject the contribution of the leaching concept; in which the Au, U, base metals and REE in the surrounding rock units has been transported by means of weathering, especially
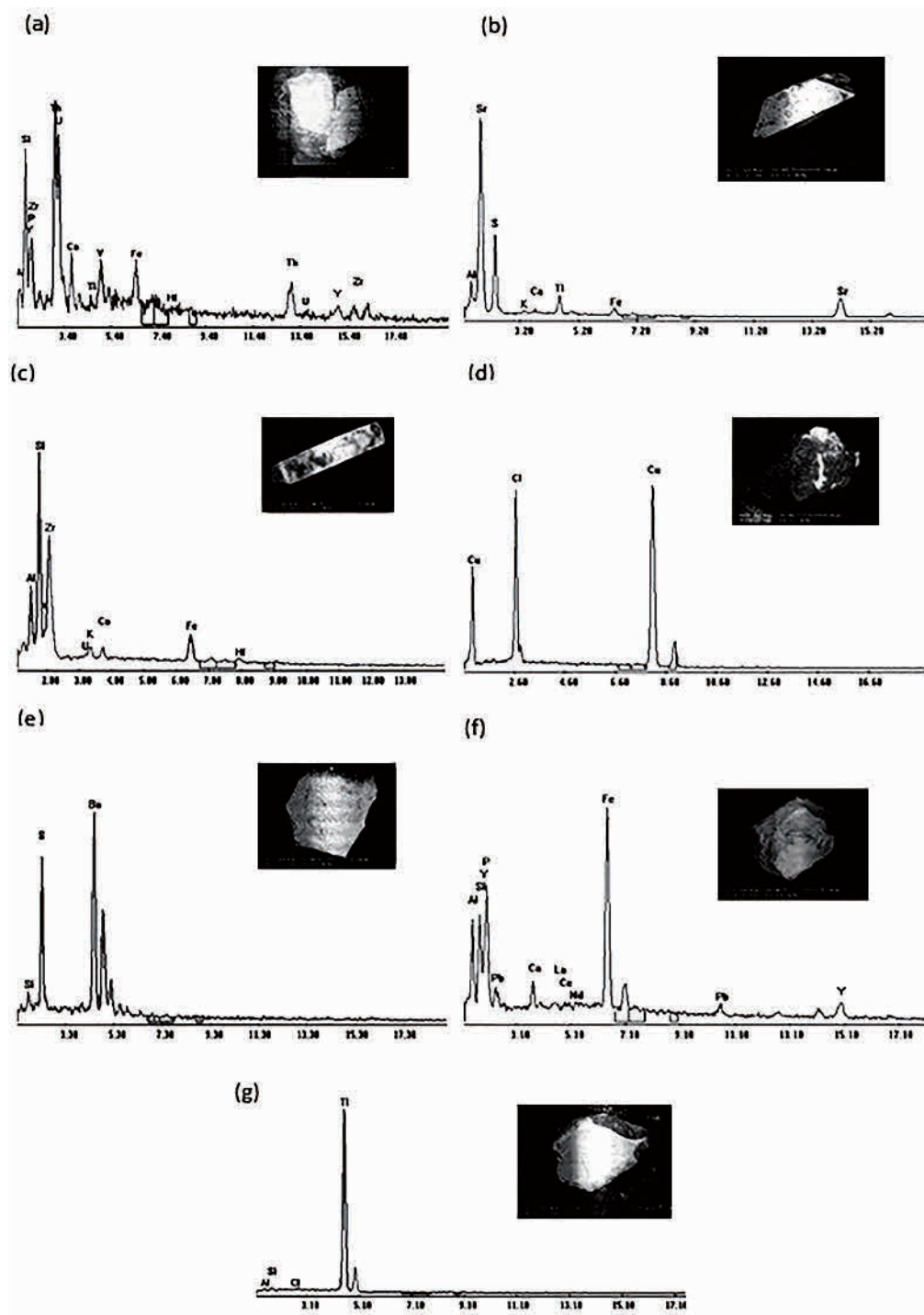
Fig. 13. EDX image showing: (a) uranothorite, (b) celestite, (c) zircon, (d) cupper, (e) barite, (f) xeno-time, (g) rutile, (representative of metal resources), Wadi Abu El Mogheirat area.

circulating water, until it is finally captured and deposited by the organic matter, in addition to the iron oxides present in the studied facies.

This preliminary study of ore deposits at Wadi Abu El Mogheirat clearly shows promising indices for the presence of valuable metals (precious metals, rare earth elements, zinc, neodymium, uranium and thorium). The most interesting lithofacies in this regard are associated with the middle Um Bogma Formation: more specifically the black gibbsite and gibbsitic marl. This 10 m-thick layer is characterized by a soft, friable structure; this is covered by a variable thickness of the semi-hard layer of the El Hashash Formation, which contains much lower contents of valuable metals. Although supplementary investigations are necessary to evaluate more precisely the spatial heterogeneity of metal distribution in the promising

rock units, these first indications clearly justify the continuation of the investigation of this promising mining area.

Acknowledgements

References

Abdelnasser, A., and Kumral, M., 2016. Mineral chemistry and geochemical behavior of hydrothermal alterations associated with mafic intrusive-related Au deposits at the Atud area, Central Eastern Desert, Egypt. Ore Geological Review, 77: 1–24.

Abu-zeid, M.M., El Kammar, A.M., El Aassy, I.E., Aly, G.A., Aita, S.K., Abu Zied, E.K., and Azeem, M.M.A., 2017. Mineral genesis and radioactivity of the upper part of the Adediya Formation, southwestern Sinai, Egypt. Ore Geological Review, 80: 536–551.

Al-Ateeq, M.A., Ahmed, A.H., Alhobaib, A.S., and Al-Saleh, A.M., 2013. Geochemistry and genesis of base metal-rich Mn-Fe mineralization in volcaniclastic sediments, Asfar Thwelil Area, Saudi Arabia. Arabian Journal of Science Engineering, 39: 361–378.

Al-Hwaiti, M., Zoheir, B., Lehmann, B., and Rabba, I., 2010. Epithermal gold mineralization at Wadi Abu Khushayba, southwestern Jordan. Ore Geological Review, 38: 101–112.

Al-Khirbash, S., Semhi, K., Richard, L., Nasir, S., and Al-Harthy, A., 2014. Rare earth element mobility during laterization of mafic rocks of the Oman ophiolite. Arabian Journal of Geosciences, 7: 5443–5454.

Alshami, A.S., 2003. Structural and lithologic control of uranium and copper mineralization in the Um Bogma environs, southwestern Sinai, Egypt. Mansoura University.

Alshami, A.S., 2019. Iinfra-cambrian placer gold-uraniferous Paleozoic sediments, southwestern Sinai, Egypt. Nuclear Sciences Scientific Journal, 8: 1–16.

Baioumy, H.M., Gilg, H.A., and Taubald, H., 2012. Mineralogy and geochemistry of the sedimentary kaolin deposits from Sinai, Egypt: Implications for control by the source rocks. Clays and Clay Minerals, 60: 633–654.

Barron, T., 1907. The Topography and Geology of the Peninsula of Sinai (Wester Portion). National Printing Department (Egypt), Cairo (Egypt).

Beyth, M., 1981. Paleozoic vertical movements in Um Bogma area, Southwestern Sinai. American Association of Petrology and Geology Bulletin, 65: 160–165.

Boskabadi, A., Pitcairn, I.K., Broman, C., Boyce, A., Teagle, D.A.H., Cooper, M.J., Azer, M.K., Mohamed, F.H., Stern, R.J., and Majka, J., 2017. Carbonate alteration of ophiolitic rocks in the Arabian-Nubian Shield of Egypt: Sources and compositions of the carbonating fluid and implications for the formation of Au deposits. International Geological Review, 59: 391–419.

Botros, N.S., 2015. Gold in Egypt: Does the future get worse or better? Ore Geology Review, 67: 189–207.

Censi, P., Saiano, F., Zuddas, P., Nicosia, A., Mazzola, S., and Raso, M., 2014. Authigenic phase formation and microbial activity control Zr, Hf, and rare earth element distributions in deep-sea brine sediments. Biogeosciences, 11: 1125–1136.

Clark, J.S.P., Peterman, Z.E., and Heier, K.S., 1966. Section 24: Abundances of uranium, thorium and potassium. In: Clark, J.S.P. (ed.), Handbook of Physical Constants. Geological Society of America.

Dawood, Y.H., Abd El-Naby, H.H., and Ghaleb, B., 2014. U-series isotopic composition of kasolite associated with aplite-pegmatite at Jabal Sayid, Hijaz region, Kingdom of Saudi Arabia. Arabian Journal of Geosciences, 7: 2881–2892.

El Aassy, I.E., El Galy, M.M., Nada, A.A., El Feky, M.G., Abd El Maksoud, T.M., Talaat, S.M., and Ibrahim, E.M., 2011. Effect of alteration processes on the distribution of radionuclides in uraniferous sedimentary rocks and their environmental impact, southwestern Sinai, Egypt. Journal of Radioanalytical and Nuclear Chemistry, 289: 173–184.

El Akeed, I.A., Sallam, O.R., Abdalla, S.A., and Mostafa, A., 2014. Polymetallic mineralization controlled by structure and lithologic factors, Wadi Sedri environ, Southwestern Sinai, Egypt. Egypt Journal of Pure and Applied Sciences, 52: 47–54.

El Kammar, A.M., ElAssay, I.E., and Abram, F.B., 1997. Rare earth elements and crystal chemistry of xenotime bearing sediments of Um Bogma area, southwestern Sinai, Egypt. Chem Erde – Geochem., 57: 91–101.

Flinter, B.H., 1959. The magnetic separation of some alluvial minerals in Malaya. American Mineralogist, 44: 738–751.

Gabr, S.S., Hassan, S.M., and Sadek, M.F., 2015. Prospecting for new gold-bearing alteration zones at El-Hoteib area, South Eastern Desert, Egypt, using remote sensing data analysis. Ore Geology Review, 71: 1–13.

Gromet, L.P., Dymekm, R.F., Haskin, L.A., and Korotev, R.L., 1984. The North-American shale composite - its compilation, major and trace-element charcateristics. Geochim Cosmochim Acta, 48: 2469–2482.

Hansink, J.P., 1976. Equilibrium analysis of sandstone rollfront uranium deposits. Proceedings Inter. Symposium on exploration of uranium deposits. Internationa. Vienna: Atomic Energy Agency, 683–693.

Haskin, L.A., Haskin, M.A., Frey, F.A. and Wildeman, T.R., 1968. Relative and Absolute Terrestrial Abundances of the Rare Earths. In: Ahrens, L.H. (ed.), Origin and Distribution of the Elements. Pergamon, 889–912.

Hassan, M.M., El Gohary, A.M. and Akarish, A.I., 2013. Preliminary record of the Proterozoic-Phanerozoic paleo-placer gold in Gebel Ghazalani area: Chemo-stratigraphic evidence closing debate about Paleozoic sedimentation sequence, east Sinai, Egypt. Egypt Journal of Geology, 57: 355–363.

Heinrich, E.W., 1958. Mineralogy and Geology of Radioactive Raw Materials. McGraw-Hill, New York (USA).

Helmy, H., and Zoheir, B., 2015. Metal and fluid sources in a potential world-class gold deposit: El-Sid mine, Egypt. International Journal of Earth Sciences, 104: 645–661.

Khalid, A.M., and Oweiss, K.A., 1995a. Results of exploration programs in Southeastern Sinai, Egypt. Annals of Geological Survey of Egypt, 20: 207–220.

Khalid, A.M., and Oweiss, K.A., 1995b. Geochemical exploration for gold at Wadi Kid area, southeastern Sinai, Egypt. Annals of Geological Survey of Egypt, 20: 333–342.

Khalifa, I.H., and Arnous, M.O., 2012. Assessment of hazardous mine waste transport in west central Sinai, using remote sensing and GIS approaches: A case study of Um Bogma area, Egypt. Arabian Journal of Geosciences, 5: 407–420.

Kora, M., Elshahat, A. and Abushabana, M., 1994. Lithostratigraphy of the manganese-bearing Um-Bogma Formation, West-Central Sinai, Egypt. Journal of African Earth Sciences, 18: 151–162.

Mitchell, A.H.G., and Garson, M.S., 1981. Mineral deposits and global tectonic settings. London: Academic Press, Inc., (U.K.)

Quinif, Y., Meon, H., and Yans, J., 2006. Nature and dating of karstic filling in the Hainaut Province (Belgium). Karstic, geodynamic and paleogeographic implications. Geodynamic Acta, 19: 73–85.

Rabeh, T., 2016. Tracing the manganese ore accumulations in Sinai Peninsula, Egypt, using magnetic method Environ Earth Sciences, 75.

Salem, S.M., Soliman, N.M., Ramadan, T.M., and Greiling, R.O., 2014. Exploration of new gold occurrences in the alteration zones at the Barramiya district, central Eastern Desert of Egypt using ASTER data and geological studies. Arabian Journal of Geosciences, 7: 1717–1731.

Sallam, O.R., Alshami, A.S., Azab, M.S., and El Akeed, I.A., 2014. Occurrence of silver-gold mineralization associated with uranium bearing minerals and base metal sulphide, El Sheik Soliman area, South Sinai, Egypt. Egypt Journal of Pure and Applied Sciences, 52: 47–54.

Schmitt, R.A., Smith, R.H., and Olehy, D.A., 1964. Rare-earth, yttrium and scandium abundances in meteoritic and terrestrial matter—II. Geochim Cosmochim Acta, 28: 67–86.

Shaaban, M.N., Holail, H.M., Sedeik, K.N., and Rashed, M.A., 2005. Multiple dolomitization events of the Lower Carboniferous Um Bogma Formation, west central Sinai, Egypt. Carbonates Evaporites, 20: 107–115.

Shata, A.E., 2006. Role of epigenetic processes in the enrichment of mineralized dolostones of the Um Bogma formation, Soutwestern Sinai, Egypt. Sedimentology of Egypt, 14: 219–242.

Shata, A.E., 2013. REE and uranium mobilization in the karst bauxites of um Bogma area, Southwest Sinai, Egypt. Sedimentology of Egypt, 20: 7–29.

Shata, A.E., and Mira, H,I., 2010. Mineralogy and geochemistry of the Mo-U-REE bearing carboniferous shale in Um Bogma area, Southwest Sinai, Egypt. Sedimentology of Egypt, 18: 11 –28.

Soliman, M.S., and Abu El Fetouh, M.A., 1969. Petrology of Carboniferous and sandstone in West Central Sinai, Egypt. Journal of Geological UAR, 13: 43–61.

Surour, A.A., El-Kammar, A.A., Arafa, E.H., and Korany, H.M., 2003. Dahab stream sediments, southeastern Sinai, Egypt: A potential source of gold, magnetite and zircon. Journal of Geochemical Exploration, 77: 25–43.

Weissbrod, T., 1969. The Paleozoic of Israel and Adjacent Countries. Part II: The Paleozoic outcrops in southwestern Sinai and their correlation with those of southern Israel. Institute for Petroleum. Research and Geophysics, Jerusalem (Israel).

Zoheir, B., and Weihed, P., 2014. Greenstone-hosted lode-gold mineralization at Dungash mine, Eastern Desert, Egypt. Journal of African Earth Sciences, 99: 165–187.